Journal of Hazardous Materials 192 (2011) 538–544

Contents lists available at ScienceDirect

Journal of Hazardous Materials

journal homepage: www.elsevier.com/locate/jhazmat

Synthesis of mesoporous BiOBr 3D microspheres and their photodecomposition for toluene

Yinchang Feng[a], Lei Li[a], Junwei Li[b], Junfeng Wang[b,*], Lu Liu[b,*]

[a] State Environmental Protection Key Laboratory of Urban Ambient Air Particulate Matter Pollution Prevention and Control, Nankai University, Tianjin 300071, PR China
[b] Tianjin Key Laboratory of Environmental Remediation and Pollution Control, Nankai University, Tianjin 300071, PR China

ARTICLE INFO

Article history:
Received 13 March 2011
Received in revised form 9 May 2011
Accepted 16 May 2011
Available online 23 May 2011

Keywords:
BiOBr
Mesoporous microspheres
Photodecomposed toluene
Degradation pathway
Computation of the electronic properties

ABSTRACT

In this article, a facile solvothermal method was introduced to synthesize mesoporous BiOBr microspheres with $Bi(NO_3)_3$ as Bi source. The synthesized catalysts were characterized by XRD, SEM, TEM, XPS, UV–vis, TG-DTA, and N_2–adsorption–desorption, and their photoactivity was evaluated by gaseous toluene both under UV and UV–vis irradiation with Degussa TiO_2 P_{25} as reference. The prepared BiOBr catalysts were of pure tetragonal phase and its band gap energy was calculated to be about 2.64 eV. Comparing with P_{25}, BiOBr showed promoted photocatalytic activity under UV–vis irradiation, during which more than 90% of toluene was eliminated after 5 h irradiation. Kinetic analysis further demonstrated the enhanced activity of BiOBr under UV–vis irradiation and the reaction rate constant *k* of BiOBr was nearly 2 times higher than that of P_{25}. The superior activity of BiOBr under UV–vis irradiation can be attributed to its hierarchical structure and suitable band gap energy. Moreover, the reacted intermediates under different light source were identified by GC–MS. Fifteen main intermediates were identified and a tentative pathway of toluene degradation by BiOBr was proposed.

1. Introduction

Volatile organic compounds (VOCs) are main indoor air pollutants, and photocatalytic oxidation is one of the most promising technologies for the removal of VOCs, during which the organic compounds are effectively oxidizing into benign and odorless constituents (H_2O and CO_2) with semiconductor and ultraviolet (UV) light or near UV light source [1–3]. Nowadays, it is still a challenge to develop new hybrid visible light responsive photocatalysts to effectively utilize visible light, which accounts for 43% of the incoming solar energy [4–6]. There are two main approaches to synthesize such visible light-driven photocatalysts. One is the chemical modification of a UV-active photocatalyst (such as, carbon doped TiO_2, Bi–TiO_2) and the other is to search novel stable materials active under visible light ($InVO_4$, $BiVO_4$, Bi_2WO_6) [4,7–9].

Bismuth oxyhalides, a group of V-VI-VII semiconductors are of great importance due to their superior optical properties and promising industrial applications, which have been used as catalysts, ferroelectric materials, pigments etc. [10,11]. For example, Bismuth oxyhalides, especially BiOCl, have industrial applications as pigments in the cosmetic industry [12]. Ai's group prepared hierarchical BiOBr microspheres by a nonaqueous sol–gel method with promoted potocatalytic performance for NO removal under visible light irradiation and they attributed the photoactivity to its special hierarchical structure [4]. Also, lamellar BiOBr prepared by Shang et al. showed excellent photoactivity for degradation of methyl orange, which is characterized by the size, the band gap, and the structure of as-prepared BiOBr catalysts [11]. Geng et al. successfully fabricated two-dimensional BiOCl lamellae via a facile sonochemical method in a surfactant/ligand-free system under ambient air [13].

In the present paper, toluene was chosen as target pollutants for three reasons as follows: (1) it is a common indoor air pollution [1,14]; (2) it has been selected as target pollutant extensively and the results are representative [15–18]; (3) due to its structural features, it is hard to be degraded, so the work has important theoretical meanings for the photocatalytic oxidation of other organic pollutants. The objective of the work is to prepare mesoporous BiOBr microspheres by solvothermal method with $Bi(NO_3)_3$ as Bi source and cetyltriethylammnonium bromide as Br source, respectively. The resultant BiOBr catalysts were well characterized and their photocatalytic activity was evaluated by photo-destruction of toluene. The relationship between the activity and the physicochemical properties of the catalyst was discussed. Furthermore, the reaction intermediates were identified by GC–MS, and a tentative degradation pathway was proposed for the first time.

* Corresponding authors. Tel.: +86 22 23503397; fax: +86 22 23503397.
E-mail addresses: jfwangnk@yahoo.com.cn (J. Wang), liul@nankai.edu.cn (L. Liu).

0304-3894/$ – see front matter
doi:10.1016/j.jhazmat.2011.05.048

2. Experiments

2.1. Preparation of the materials

The BiOBr catalysts were synthesized via a facile solvothermal method. Typically, 0.3 g $Bi(NO_3)_3$ was dissolved in 10 mL absolute ethanol, and 0.6 g cetyltriethylammnonium bromide (CTAB) was added very slowly to the solution. The solution was stirred and sonicated for 10 min, during which a white precipitate was formed. The precipitate was transferred to a 50-mL Teflon-lined autoclave, and the autoclave was further filled with absolute ethanol to 80% of its total volume. The autoclave was sealed and heated at 150 °C for 24 h. After cooling down to room temperature, the obtained products were collected and washed with deionized water and absolute ethanol several times, and finally dried at in the air for further use. All chemicals were of analytical grade and used as received without further purification.

2.2. Characterization

X-ray diffraction (XRD) patterns were obtained on a Rigaku D/Max-2500 diffractometer with Cu Kα radiation (λ = 1.54178 Å). The morphology and size of the synthesized catalysts were recorded by field emission scanning electron microscope (FESEM, FEI nanosem 430) and high-resolution transmission electron microscope (HRTEM, Tecnai G^2F 20), respectively. The UV–vis diffuse reflectance spectra (UV–vis DRS) were performed at room temperature by a SHIMADZU UV-3600 spectrophotometer equipped with an integrated sphere and using $BaSO_4$ as reference. The specific surface area were calculated using a Quantachrome NOVA 2000e sorption analyzer at 77 K with samples degassed at 120 °C under vacuum prior to test. X-ray photoemission spectroscopy (XPS) was measured using a Kratos Axis Ultra DLD spectrometer employing a monochromated Al Kα X-ray source ($h\nu$ = 1486.6 eV). All XPS spectra were recorded using an aperture slot of 300 μm × 700 μm, survey spectra were recorded with a pass energy of 160 eV, and high resolution spectra with a pass energy of 40 eV. Thermogravimetric analysis was studied by a Rigaku-10 A thermogravimatric-differential thermal analyser. Each sample was treated under air and heated from room temperature to 800 °C at a rate of 10 °C/min.

2.3. Photocatalytic measurements and Reaction intermediates identification

The photocatalytic degradation experiments of gaseous toluene over BiOBr microspheres were carried out in a photochemical reactor, which is consisted by a cylindrical quartz reactor with an effective volume of 1 L, a cooling water system, a light source horizontally positioned up the reactor, and a port at the top of the photoreactor for measuring temperature, relative humidity and withdrawing toluene reacted samples (Supporting information Fig. S1). A 300 W ultraviolet Hg lamp and a 350 W Xenon lamp, simulating solar light radiation (Institute of Electric Light Source, Beijing) were selected as the UV and UV–vis light source, respectively. Typically, 0.5 g catalysts were dispersed in 10 mL absolute ethanol, and the resultant suspension was treated by ultrasonic technique for 30 min to achieve complete distribution of the catalysts. Then, the suspension was uniformly loaded on the inside of the whole reactor (the top of the reactor being not included), after which the catalysts were uniformly supported in the reactor. To minimize the effect of absolute ethanol in the process, the treated reactor was heated in the oven at 40 °C for 30 min. The coated reactor was sealed with medical absorbent cotton, parafilm and silica gel stopper. Previous experiments indicated that there was no change in toluene concentration by the seal process within 8 h. Static vacuum gas distribution was adopted to obtain certain amount of gaseous toluene in the photocatalysts coated reactor. Approximately, the coated reactor reached vacuum by a vacuum pump, and 10 μL toluene was injected to it through the silica gel stopper. Air having been treated by activated carbon fiber was introduced into the reactor through the external tube and the preparation process was finished. Prior to the irradiation, the toluene vapor was allowed to achieve gas–solid adsorption equilibrium with the coated catalysts for 2 h. Based on our previous experimental data, less than 10% of toluene was adsorbed on the coated catalysts during the adsorption process, implying that photocatalytic oxidation was the main reason for removing the target pollutant. Then, the light was switched on and the photocatalytic reaction was started. The reacted gaseous samples were withdrawn at regular time intervals by a 50 μL gastight pressure-lock precision analytical syringe (Hamilton, Switzerland) and measured with an Agilent 6820 gas chromatograph equipped with a FID detector and a HP-5MS capillary column (0.25 mm i.d.×30 m). Toluene conversion was calculated by the following equation:

$$\text{Conversion}\,(\%) = \left(\frac{C_0 - C_t}{C_0}\right) \times 100\%$$

where C_0 and C_t represents the toluene initial adsorption equilibrium concentration and reaction concentration, respectively. The temperature in the reactor was almost as the same as the room temperature, and the inside humidity was ranging from 20% to 30%, which changed little during the entire photocatalytic process. Blank experiment without catalyst under identical conditions was conducted to exclude the influence of photolysis on toluene conversion. All experiments were performed in triplicate. The whole experiment (sampling and analysis) was measured with P_{25} six times and the resulting relative standard deviation was within 5%. The adsorbed reacted intermediates were identified by GC–MS after methanol extraction. The mixture of the used catalyst and methanol was ultrasonic for 15 min, then centrifuged for 15 min with 3000 rpm and the obtained supernatant was concentrated by rotary evaporation methods and nitrogen-blow methods. The condensed solution was directly analyzed by GC–MS (Aglient 6890, USA) equipped with a HP-5MS capillary column and m/z scanning from 45 to 260, with nitrogen as carrier gas. MS identification was based on both the reported literatures referring toluene photocatalytic oxidation and NIST 05 library with a fit higher than 90%.

3. Results and discussions

3.1. Preparation of the materials

X-ray diffraction (XRD) was recorded to investigate the phase structure of the as-prepared powders. Fig. 1 shows the XRD patterns of the fresh and reacted BiOBr microspheres. All the diffraction peaks can be well indexed to crystallized pure tetragonal phase with lattice constants of $a = b$ = 30926 Å, c = 8.103 Å (JCPDS Card NO. 09-0393). No other diffraction peaks are found, indicating the high purity and single-phase of the prepared samples. Comparing the XRD patterns of the fresh and reacted BiOBr, there is no phase change, which suggests the stability of the synthesized BiOBr catalysts. However, the diffraction peaks of the reacted catalysts are weaker, and this can be ascribed to the formation of the non-crystal materials on the surface of the catalysts (the organic intermediates).

The SEM images of the resulting products are presented in Fig. 2. The low-magnification pictures in Fig. 2 indicate that the fabricated BiOBr is flower-like microshperes with diameters about 2 μm and the microspheres are composed of many radially grown nanosheets with a thickness of about 25 nm (high-magnification pictures). During the photocatalytic process, the thin nanosheets are beneficial for improving the separating efficiency of the electron–hole and

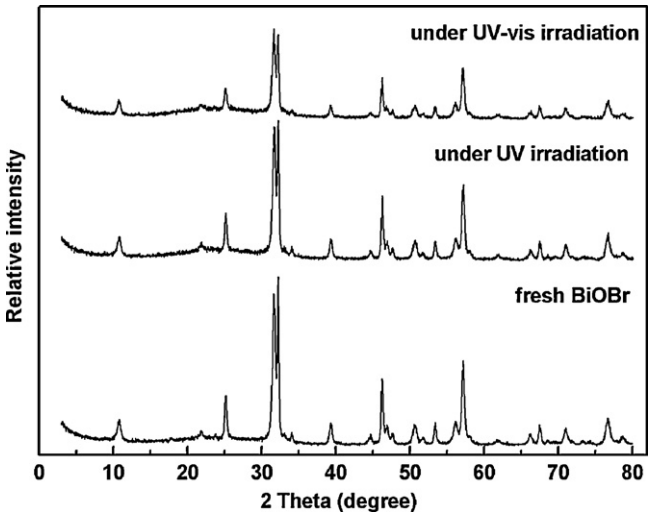

Fig. 1. XRD patterns of the fresh and reacted BiOBr microspheres.

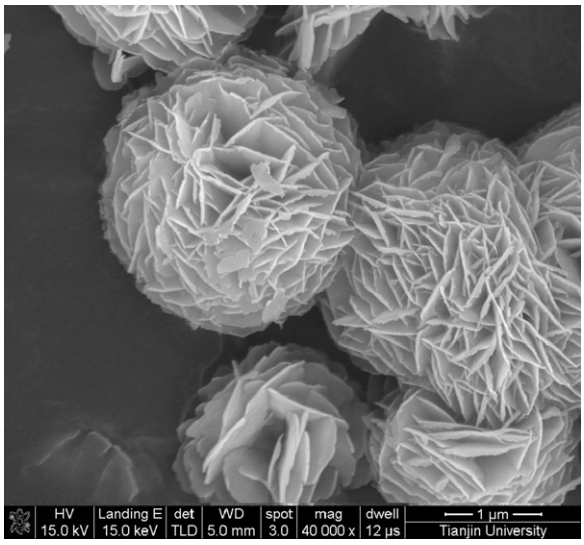

Fig. 3. SEM images of the BiOBr microspheres (before photocatalytic reaction).

resulting in high phtocatalytic performance. As it is shown in Fig. 3, there is no difference in morphology and size of the catalysts before and after photocatalytic reaction.

UV–vis diffuse reflectance spectra (DRS) of the BiOBr microspheres and P_{25} are given in Fig. 4. As a crystalline semiconductor, the optical absorption near the band edge follows the formula $\alpha h\nu = A(h\nu - E_g)^{n/2}$, where α, ν, E_g, and A are the absorption coefficient, light frequency, band gap energy, and a constant, respectively [8]. Therefore, the band gap of the BiOBr microspheres is estimated to be 2.64 eV, which is a key factor in determining its photocatalytic activity and is close to the value reported in other literatures (P_{25} is about 3.2 eV) [11]. Comparing with P_{25}, the formulated BiOBr microspheres exhibits a sharp increase absorption in the UV–vis region, which allows the BiOBr catalysts to utilize more light during photocatalytic degradation and is expected to enhance the photocatalytic behavior [4]. The steep shape of the visible edge and the strong absorption in the visible region of the BiOBr microspheres can be attributed to the intrinsic transition between the valence band and the conduction band, instead of transition from the impurity to the conduction band [5]. We computed the electronic properties of BiOBr in the framework of density functional theory (DFT) by employing the generalized gradient approximation (GGA) with the PW91 functional and the double numerical plus polarization (DNP) basis set implemented in the DMol^3 pack-

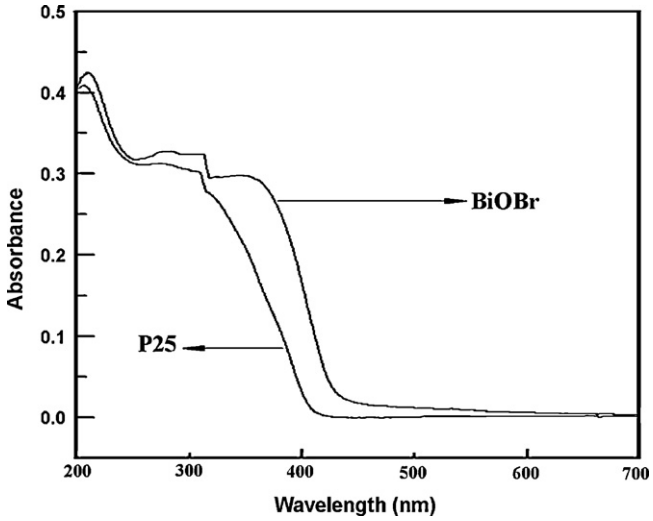

Fig. 4. UV–vis spectra of P_{25} and the prepared BiOBr microspheres.

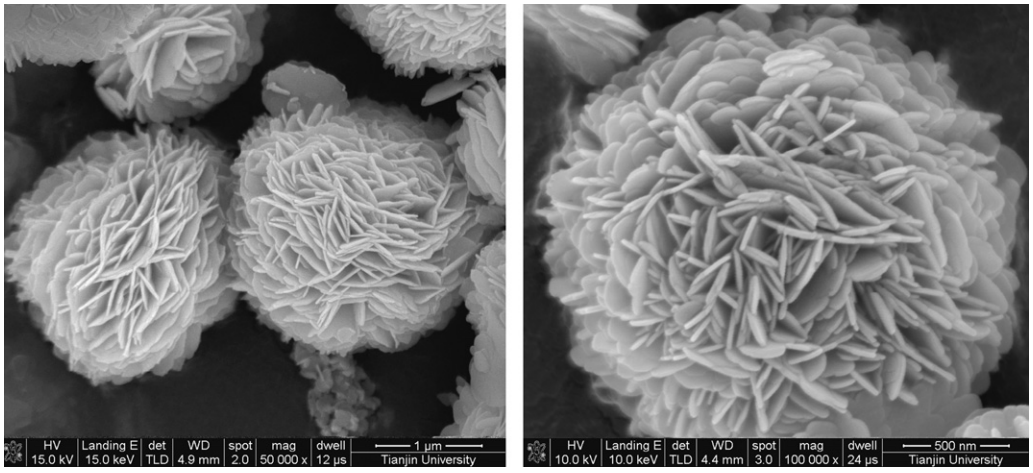

Fig. 2. SEM images of the BiOBr microspheres (after photocatalytic reaction).

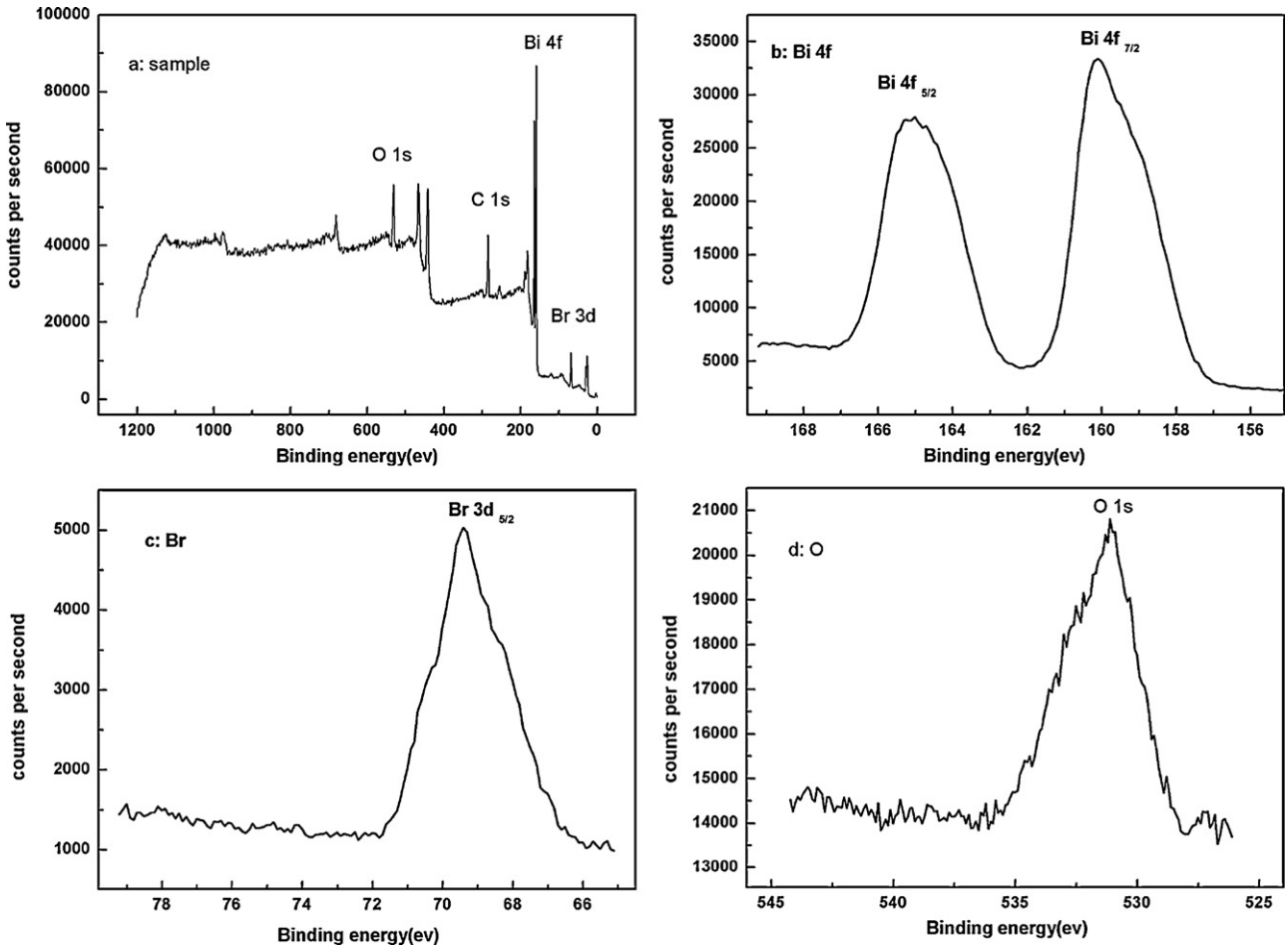

Fig. 5. XPS spectrum of the synthesized BiOBr microspheres.

age, which reveals that ehe valence band maximum (VBM) of BiOBr mainly comes from the 6p electrons of Bi, while the conduction band minimum (CBM) consists mainly of Br-4p and O-2p orbitals [19,20].

X-ray Photoelectron Spectroscopy (XPS) was applied to investigate the surface element composition of the BiOBr samples and the results are provided in Fig. 5. The survey XPS spectrum reveals that the sample is constituted by elements of Bi, O, Br and C. It can be observed that the spin orbit splitting peaks of Bi 4f level is split into two peaks centered at 165.0 and 160.1 eV, which belong to the Bi 4f5/2 and Bi 4f7/2, respectively. So the main chemical states of Bismuth element in the samples are tri-valence. The carbon peak can be attributed to the adventitious elemental carbon on the surface of the sample from atmosphere. Further investigations demonstrated that there is no element difference between the fresh and reacted samples, which can be seen in supporting information Fig. S2.

N_2 adsorption–desorption technique was carried out to investigate the pore structure and surface area of the mesoporous BiOBr microspheres, and the results are given in Fig. 6. According to the IUPAC classification, the isotherm can be classified to the typical IV pattern, which is characterized with a hysteresis loop. The surface area, pore volume and the pore size of BiOBr are calculated to be 5.3 m^2/g, 0.02 mL/g and 15.0 nm. The large pore size can be due to its flower-like structure, which is beneficial for the diffusion of reactants and intermediates during reaction. Also the TG and DTA curves of the BiOBr microspheres are presented in supporting information Fig. S3. There is no weight loss below the temperature of 500 °C, so the prepared samples are of good stability and purity under the reacted temperature (room temperature).

3.2. Photocatalytic degradation of toluene

In order to determine the photocatalytic ability of the BiOBr microspheres and investigate the effect of various light sources on its photocatalytic performance, a series of experiments for toluene degradation under UV or UV–vis irradiation were carried out at room temperature and the experimental results are shown in Fig. 7.

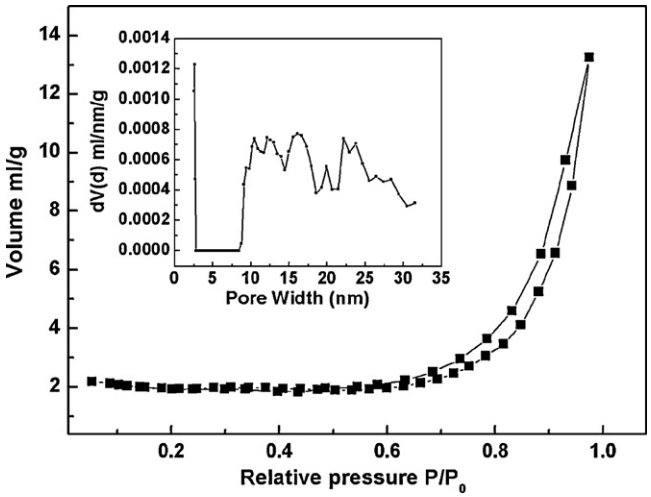

Fig. 6. N_2 adsorption–desorption isotherms and pore size distribution of the BiOBr microspheres.

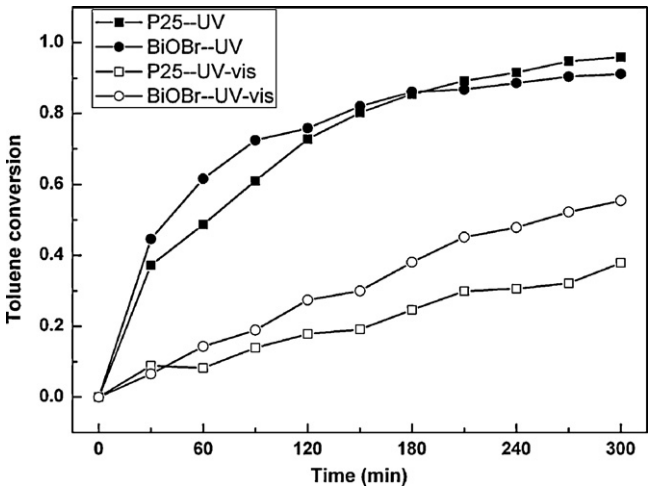

Fig. 7. Toluene conversion versus illumination time with P_{25} and the BiOBr microspheres under various irradiaton sources.

Table 1
The reaction rate constants and their corresponding R^2 using P_{25} and BiOBr under various irradiation sources.

	UV	UV–vis
P_{25}	$K = 0.0105\ (min^{-1})$ $R^2 = 0.9974$	$K = 0.0015\ (min^{-1})$ $R^2 = 0.9812$
BiOBr	$K = 0.0073\ (min^{-1})$ $R^2 = 0.9369$	$K = 0.0028\ (min^{-1})$ $R^2 = 0.9947$

The reaction rate constant k follows the pseudo-first-order reaction [21,7] and the equation can be expressed as follows:

$$\ln \frac{c_0}{c_t} = kt$$

where c_0 and c_t is the initial toluene equilibrium concentration and reaction concentration, respectively, and t is the reaction time (min). The reaction rate constants are listed in Table 1. As our previous experiments demonstrated, direct photolysis has little effect on toluene degradation. The reaction rate constant k of P_{25} is a little higher than that of BiOBr under UV irradiation, while k of BiOBr is about a 2-fold increase as that of P_{25} under UV–vis irradiation. The photorcatalytic performance is determined by both the size and morphology of the photocatalysts. The flower-like hierarchial structure can supply more active sites and is beneficial for the diffusion of intermediates during reaction, thus enhancing the

Table 2
The identified possible absorbed reacted intermediates.

Compounds	Retention time	*m/z*	Structural formula
Cyclohexanone	6.93, 6.95, 7.13	98	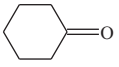
Cyclohexene, 1-methoxy-	7.493	112	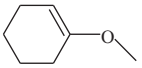
Benzaldehyde	8.40, 8.534	106	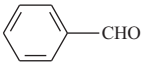
Phenol	9.022	94	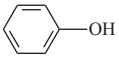
Cyclohexane,1,1-dimethoxy-	9.439	144	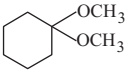
Benzyl alcohol	9.973	108	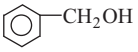
Benzoic acid, methyl ester	11.029	136	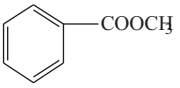
Benzaldehyde dimethyl acetal	11.295	152	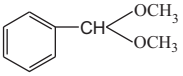
Benzenecarboxylic acid	12.11, 12.377, 12.477, 12.558	122	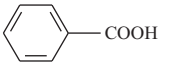
Benzaldehyde, -bromo-	12.98	184	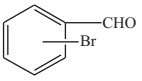
Benzoic acid, butyl ester	15.168	178	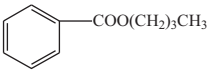
Dimethyl phthalate	16.23	194	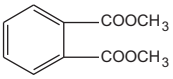
1,4-Benzenedicarboxylic acid, dimethyl ester	16.788	194	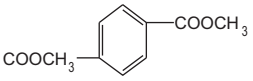
Dibutyl phthalate	21.360	278	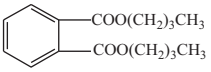

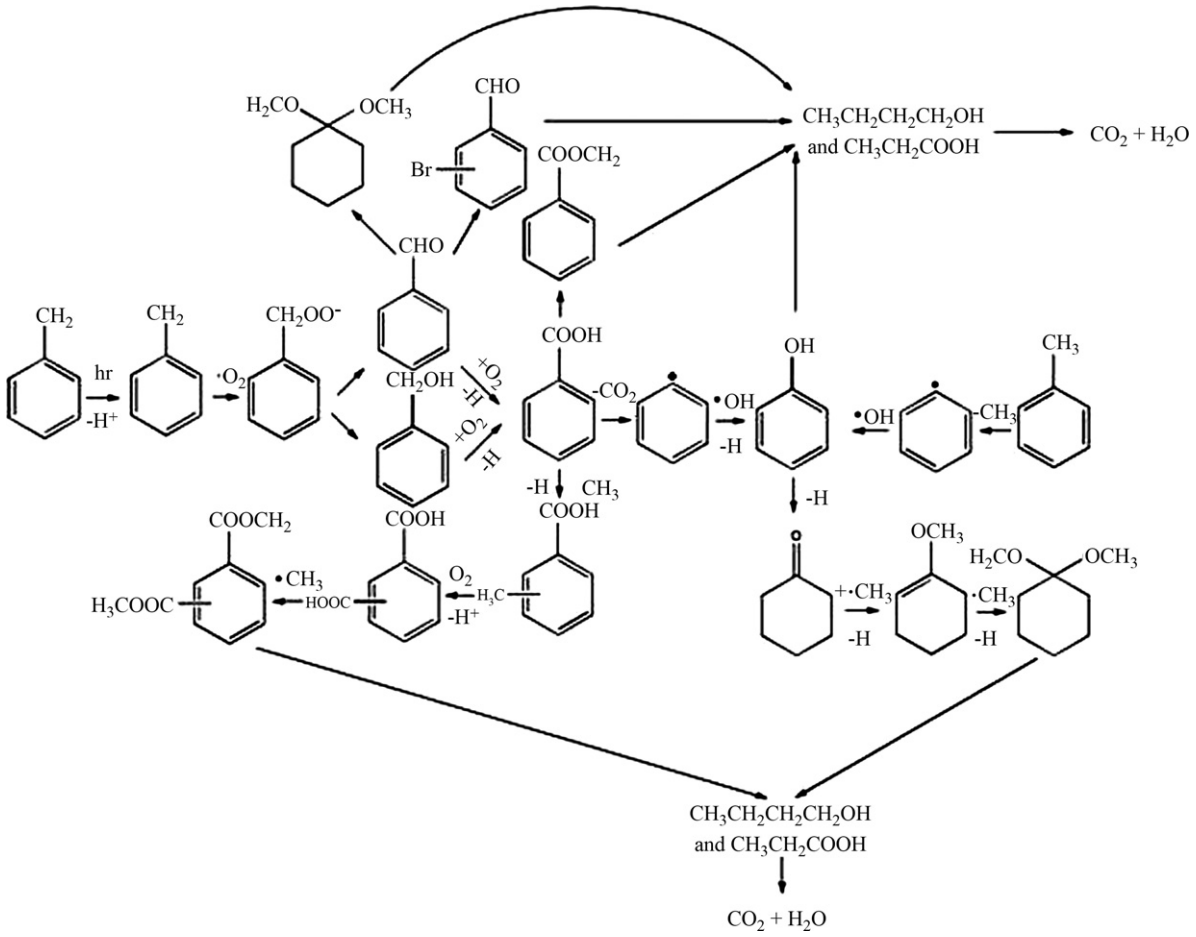

Fig. 8. The proposed degradation process of toluene.

adsorption of pollutants and leading to higher photoactivity [5]. The experimental UV–vis data revealed that the BiOBr microspheres prefer to absorbing visible light than P_{25}. Meanwhile, because of its more positive VB than P_{25} (the O_2/H_2O potential level is +1.23 eV), the BiOBr can split water into O_2, which can promote the photocatalysis process. When under UV–vis irradiation, BiOBr showed much superior performance than P_{25}, which may be derived from its ability to absorbing visible light and its structure by supplying more active sites for toluene and diffusing reaction intermediates [4,22,23].

3.3. Intermediates analysis

During the whole photocatalytic process, the formed intermediates can adsorb on the surface of the catalysts and inhabit the active sites, thereby influencing the whole reaction and even resulting the deactivation of the photocatalyst [24,25]. Meanwhile, the newly formed intermediates may be much more dangerous, toxic or stable than the starting material, and become extra contaminative sources [26]. So it is imperative to investigate the reaction intermediates. GC–MS was employed to identify the absorbed reaction intermediates formed under different irradiation sources and the possible intermediates are listed in Table 2 in detail (GC–MS results seeing supporting information Fig. S4). There is no difference in intermediates between the UV and UV–vis light source with BiOBr as photocatalyst (supporting information Fig. S4). Benzaldehyde, benzyl alcohol and benzenecarboxylic acid were detected in all the experiments in spite of the catalysts or the light source adopted. Comparing the reaction products, some hydroxyl-related products, such as benzaldehyde, 2-hydroxy were identified on the surface of the reacted P_{25}, which can be attributed to the facile fomation of hydroxyl radicals during reaction by P_{25}. During the whole photocatalytic oxidation process, the hydroxyl radicals can enhance the photocatalytic reaction or compete the adsorption sites with the pollutants [26], so the relative superior toluene conversion rate by P_{25} may be with the formation of those radicals. On the other hand, there are many complex and toxic intermediates: for example cyclohexanone, phenol, 1,1-dimethoxy-cyclohexane, Benzoic acid, methyl ester, Benzaldehyde dimethyl acetal, Dimethyl phthalate, 1,4-Benzenedicarboxylic acid, dimethyl ester, Propanoic acid, 2-methyl-,1-(1,1-dimeth ylethyl)-2–methyl-1,3-propanediyl ester, dibutyl phthalate, detected on the BiOBr surface, which need further investigation for evaluating the whole process. The oxidation process probably proceeded in the following sequence: toluene – benzyl alcohol – benzaldehyde – benzoic acid. The highly stable aromatic ring of toluene is intact when the active methyl group of the toluene molecule is oxidized step-by-step to benzoic acid. The formation of the carbonyl group makes the benzyl ring even more inert because the conjugation effect of the carbonyl group reduces the electron density of the benzyl ring, however, benzoic acid methyl ester, dimethyl phthalate, etc. intermediates formed lead to the conjugation structure is unstable and undergoes a fast opening of the aromatic ring, and forming aliphatic compounds such as $CH_3CH_2CH_2CH_2OH$, $CH_3CH_2CH_2OH$. The complete oxidation products, such as CO_2 and water, come from the intermediates when the benzyl ring is broken. Fig. 8 illustrates the photodegradative pathway of toluene in the BiOBr–UV system.

4. Conclusion

In summary, mesoporous used BiOBr microspheres were synthesized via a simple solvothermal route. The surface area, pore volume and the pore size of the BiOBr microspheres are 5.3 m^2/g, 0.02 mL/g and 15.0 nm, respectively. The bang gap energy of BiOBr was estimated to be about 2.64 eV by the UV–vis diffuse reflectance spectra, and BiOBr showed obvious absorption in the visible region, which can be attributed to the intrinsic transition between the valence band and the conduction band. A series of experiments for toluene degradation under UV or UV–vis irradiation were carried out at room temperature. Toluene conversion of BiOBr is almost the same with P_{25} under UV irradiation. However, it was enhanced when BiOBr was added as catalysts under UV–vis irradiation, with k of BiOBr was about 2 times than P_{25}. The superior activity of BiOBr under UV–vis irradiation can be attributed to its flower-like structure and suitable band gap energy. GC–MS was applied to identify the reaction intermediates formed under different irradiation sources and the possible intermediates. There is no difference in intermediates between the UV and UV–vis light source with BiOBr as photocatalyst, and fifteen main intermediates have been identified provided that it was followed the procedure described above.

Acknowledgments

This research was supported by 2008 National Science Foundation of China (no. 20877042), and China-US Center for Environmental Remediation and Sustainable Development.

Appendix A. Supplementary data

Supplementary data associated with this article can be found, in the online version, at doi:10.1016/j.jhazmat.2011.05.048.

References

[1] G. Martra, S. Coluccia, L. Marchese, V. Augugliaro, V. Loddo, L. Palmisano, M. Schiavello, Catal. Today 53 (1999) 695–702.
[2] J. Jeong, K. Sekiguchi, K. Sakamoto, Chemosphere 57 (2004) 663–671.
[3] A.J. Maira, J.M. Coronado, V. Augugliaro, K.L. Yeung, J.C. Conesa, J. Soria, J. Catal. 202 (2001) 413–420.
[4] Z. Ai, W. Ho, Z. Lee, L. Zhang, Environ. Sci. Technol. 43 (2009) 4143–4150.
[5] J. Zhang, F. Shi, J. Lin, D. Chen, J. Gao, Z. Huang, X. Ding, C. Tang, Chem. Mater. 20 (2008) 2937–2941.
[6] Z. Jiang, F. Yang, G. Yang, L. Kong, M.O. Jones, T. Xiao, P.P. Edwards, J. Photochem. Photobiol. 212 (2010) 8–13.
[7] F. Dong, H. Wang, Z. Wu, J. Phys. Chem. C 113 (2009) 16717–16723.
[8] X. Zhang, F. Jia, L. Zhang, J. Phys. Chem. C 112 (2008) 747–753.
[9] X. Chang, J. Huang, C. Cheng, Q. Sui, W. Sha, G. Ji, S. Deng, G. Yu, Catal. Commun. 11 (2010) 460–464.
[10] Z. Deng, D. Chen, B. Peng, F. Tang, Cryst. Growth Des. 8 (2008) 2995–3003.
[11] M. Shang, W. Wang, L. Zhang, J. Hazard. Mater. 167 (2009) 803–809.
[12] J. Henle, P. Simon, A. Frenzel, S. Scholz, S. Kaskel, Chem. Mater. 19 (2007) 366–373.
[13] J. Geng, W. Hou, Y. Lv, J. Zhu, H. Chen, Inorg. Chem. 44 (2005) 8503–8509.
[14] V. Augugliaro, S. Coluccia, V. Loddo, L. Marchese, G. Martra, L. Palmisano, M. Schiavello, Appl. Catal., B 20 (1999) 15–27.
[15] A.J. Maira, K.L. Yeung, J. Soria, J.M. Coronado, C. Belver, C.Y. Lee, V. Augugliaro, Appl. Catal., B 29 (2001) 327–336.
[16] F.B. Li, X.Z. Li, C.H. Ao, S.C. Lee, M.F. Hou, Chemosphere 59 (2005) 787–800.
[17] M.D. Hernández-Alonso, A.B. Hungrĩıa, A. Martĩınez-Arias, M. Fernández-Garcĩıa, J.M. Coronado1, J.C. Conesa, J. Soria, Appl. Catal., B 50 (2004) 167–175.
[18] F. Bosc, D. Edwards, N. Keller, V. Keller, A. Ayral, Thin Solid Films 495 (2006) 272–279.
[19] W.L. Huang, Q.S. Zhu, Comput. Mater. Sci. 43 (2008) 1101–1108.
[20] W.L. Huang, Q.S. Zhu, Comput. Mater. Sci. 46 (2009) 1076–1084.
[21] M. Zhou, J. Yu, S. Liu, P. Zhai, B. Huang, Appl. Catal., B 89 (2009) 160–166.
[22] J. Yu, M. Zhou, B. Cheng, H. Yu, X. Zhao, J. Mol. Catal. A: Chem. 227 (2005) 75–80.
[23] A. Kar, Y. Smith, V. Subramanian, Environ. Sci. Technol. 43 (2009) 3260–3265.
[24] M.C. Blount, J.L. Falconer, Appl. Catal., B 39 (2002) 39–50.
[25] J.M. Coronado, S. Kataoka, I. Tejedor-Tejedor, M.A. Anderson, J. Catal. 219 (2003) 219–230.
[26] M. Sleiman, P. Conchon, C. Ferronato, J. Chovelon, Appl. Catal., B 86 (2009) 159–165.